Effectiveness Evaluation of the Measures for Improving Resilience of Nuclear Structures against Excessive Earthquake (1) Fragility Evaluation of Reactor Vessel based on Structural Analysis

Hiroyuki Nishino[a*], Kenichi Kurisaka[a], Satoshi Futagami[a], Tomoyoshi Watakabe[a], Hidemasa Yamano[a],

[a] Japan Atomic Energy Agency, Oarai, Japan

Abstract: The reactor vessel (RV) buckling was a dominant contributor to core damage. However, even if the RV is buckled due to seismic shaking, it is expected that the RV maintains stable state without unstable failure such as rupture, collapse. Realistic consideration of the post-buckling behavior is regarded as a measure for improving the resilience in this study. The purpose of this study is to understand the post-buckling deformation behavior of the RV and to evaluate the RV fragility based on fatigue failure. This study performed structural analysis using a finite element method to quantify time histories of displacement, strain, etc. As the result of the analysis, wrinkles of the buckling appeared at the elevation higher than the liquid level in the RV. The largest strain value was also indicated around this elevation. The cumulative fatigue damage fraction was evaluated in this analysis to evaluate the fragility of fatigue failure in addition to the buckling fragility. The result showed that the seismic intensity for the median fragility of the fatigue failure was about six times larger than the design-basis ground motion. This is 1.2 times larger than the buckling-based result, which suggests that realistic evaluation of the post-buckling behavior could contribute to improving the resilience of the nuclear structure.

Keywords: Excessive earthquake, Fragility evaluation, Cumulative fatigue failure fractions, Sodium-cooled Fast Reactors, Probabilistic Risk Assessment.

1. INTRODUCTION

Japan Atomic Energy Agency (JAEA) has been implementing research and development for seismic probabilistic risk assessment (PRA) of sodium-cooled fast reactors (SFR), in which a horizontal seismic isolation system is installed in the building. In the past PRA study, the seismic failure of the structures, systems and components was evaluated based on the design limits, i.e., buckling for reactor vessel (RV) and shell of intermediate heat exchangers, bending failure for piping. The RV buckling was a dominant contributor to core damage and it could occur when the seismic intensity increases to the hardening behavior region of the laminated rubber bearings. However, even if the RV is buckled due to seismic shaking, it is expected that the RV maintains stable state without unstable failure such as rupture, collapse. Realistic consideration of the post-buckling behavior should be taken as a measure for improving the resilience in this study.

The purpose of this study is to understand the post-buckling deformation behavior of the RV and to evaluate the RV fragility based on fatigue failure. As a preliminary analysis, the behavior was analyzed and RV fragility was evaluated by using only the horizontal seismic wave in previous study [1]. The present study implements analysis of the behavior and evaluation of the RV fragility based on fatigue failure by using not only horizontal seismic wave but also vertical one.

2. FLOW OF FRAGILITY EVALUATION

This study evaluates the fragility evaluation according to Fig.1. First step is to set the structural analytical conditions and waveforms of seismic floor response at the RV location for various intensities of seismic ground motion. This first step is implemented in Section 3. Second step is to analyze detailed three-dimensional structural analysis of the RV by a finite element method and to quantify time histories of displacement, strain, etc. Third step is to implement the zooming analysis by focusing attention on the buckling and the structural deformation of RV. Fourth step is to calculate the cumulative fatigue damage fraction: Df by using result of these structural analyses. These second, third and fourth steps are implemented in Section 4. Last step is to evaluate the fragility by applying the safety factor method using response factor of the building and components, capacity factor and their uncertainties. The last step is implemented in Section 5.

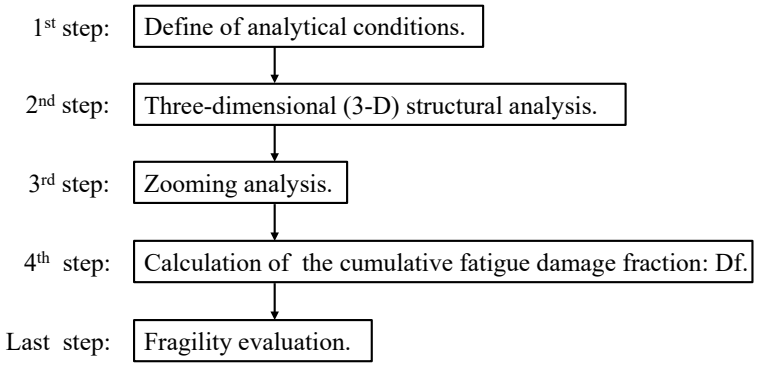

Figure 1. Flow of Fragility Evaluation

3. ANALYTICAL CONDITIONS

Figure 2 shows the loop-type SFR. The reactor building of the SFR has horizontal seismic isolation system which consists of laminated rubber bearings and oil damper. This study implements structural analysis for the SFR, where the setup for the analysis is same as previous study [1] as follows.

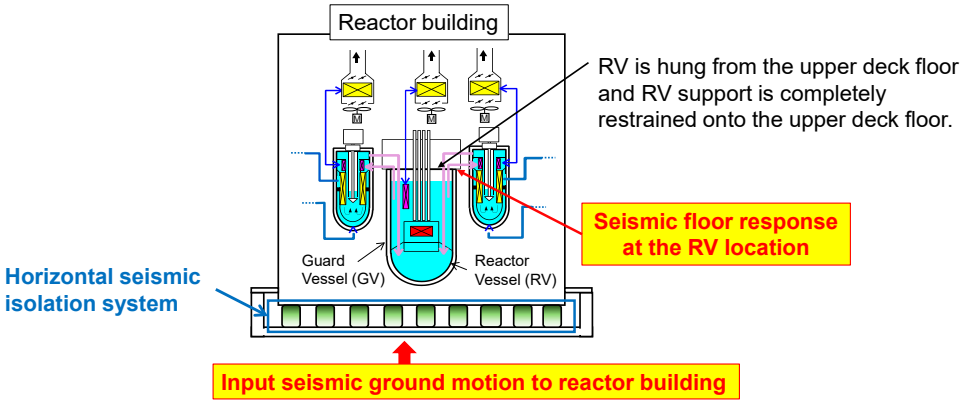

Figure 2. Relation of Reactor and Horizontal Seismic Isolation System

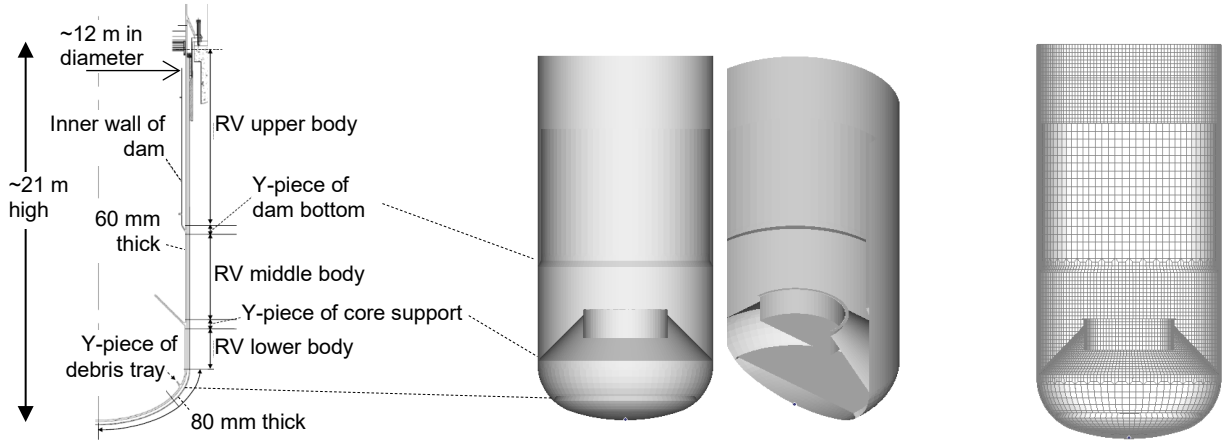

(a) Reactor Vessel (RV) (b) Three-Dimensional Modelling (c) Meshing

Figure 3. Analytical Geometry

The structural analysis of the RV used a commercially available finite element analysis code, FINAS/STAR. As drawn in Fig. 3, only the RV is modelled in this paper to avoid the interaction with a guard vessel (GV), which covers the RV in the design. A three-dimensional geometry is expressed by shell elements. The RV material is 316FR stainless steel [2]. The RV height is about 21,000 mm. The inner diameter and thickness of

the RV body are about 12,000 mm and 60 mm, respectively. The thickness of the RV lower part is 80 mm. The masses of the RV, the reactor internal structure, and the core assemblies are 514 tons, 554 tons, and 454 tons, respectively. The RV is hung from the upper deck floor. This analysis assumed that the RV support was completely restrained onto the upper deck floor. Based on these conditions, the structural analysis used several multipliers of the design-basis ground motion conditions, i.e., 1, 5, 5.5, 6, 6.2 and 6.3.

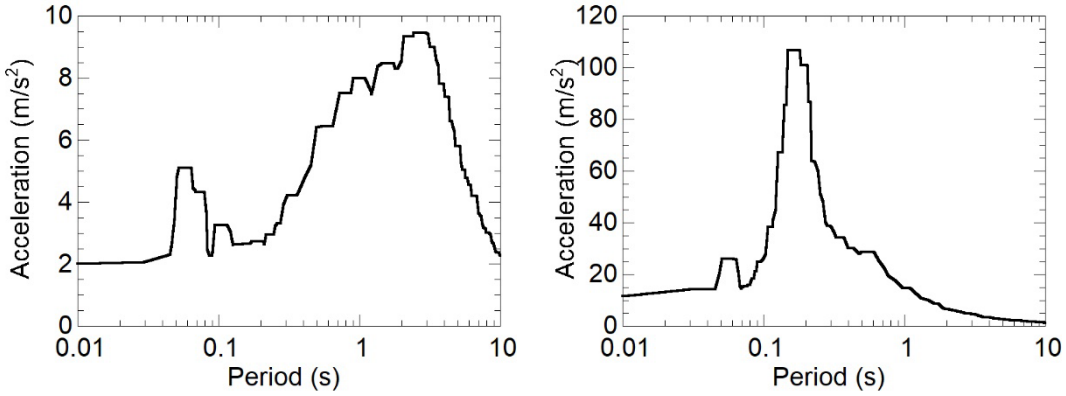

(a) Horizontal Direction (b) Vertical Direction

Figure 4. Floor Response Spectra of Design-Basis Ground Motion

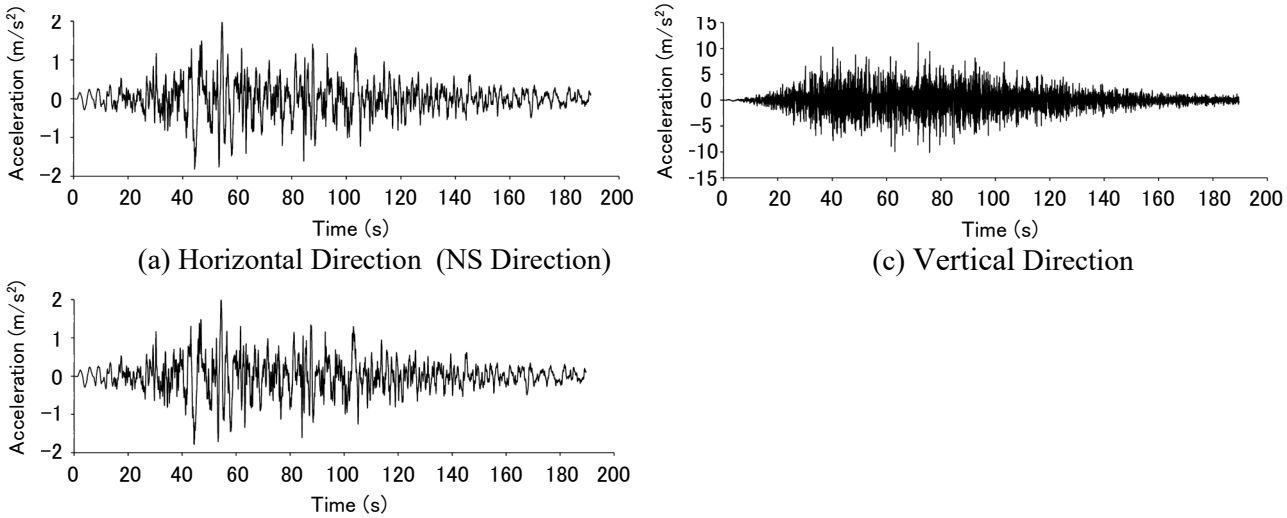

(a) Horizontal Direction (NS Direction) (c) Vertical Direction

(b) Horizontal Direction (EW Direction)

Figure 5. Waveforms of Design-Basis Seismic Floor Response

By using same method in previous study [1], this study defined a design basis seismic condition, which has been separately carried out for a horizontal seismic isolation system for the next generation fast reactor [3]. The maximum accelerations are ~800 gal (8 m/s^2) in a horizontal direction and 533 gal in the vertical direction. Using this condition input to the reactor building, a condition of design-basis seismic floor response at the RV location was obtained by a floor response analysis [3]. Figure 4 shows spectra of the design-basis seismic floor response at the RV location. The acceleration is low at the natural frequency, which is ~5 Hz (~0.2 s) in the horizontal and ~10 Hz (~0.1 s) in the vertical direction. It should be noted that the vertical acceleration is significantly high. Using these spectra, the waveforms of design-basis seismic floor response were created separately from this study. Figure 5 shows the waveforms of design-basis seismic floor response in the North-South (NS) , East-West (EW) directions and vertical direction. This study multiplied the amplitude of the design-basis condition by factors to develop a fragility curve of the RV.

4. STRUCTURAL ANALYSIS

4.1 Relation of Input Seismic Ground Motion to Reactor Building and Seismic Floor Response at RV Location

Figure 2 shows the image for relation of input seismic ground motion to reactor building and seismic floor response at RV location. The seismic floor response at RV location shakes RV support restrained onto the upper deck floor. The nonlinear characteristic of the floor response appears when the seismic condition is greater than the design-basis ground motion in the seismic isolation system [4]. This study developed a regression line of the power math function to express the relationship between the input seismic ground motion to the reactor building and the seismic floor response at the RV location in the following equations.

Horizontal direction:

$$LN(m) = 0.1292 \cdot LN(n)^2 + 1.015 \cdot LN(n) - 0.0006 \quad (1)$$

Vertical direction:

$$LN(m) = 0.1147 \cdot LN(n)^2 + 1.325 \cdot LN(n) - 0.0089 \quad (2)$$

where m is the multiplier of the design-basis seismic floor response at the RV location, and n is the multiplier of the input design-basis ground motion to the reactor building. As condition for using these equations, this study assumed that the horizontal seismic isolation system installed at the building is designed to prevent failure caused by the building locking behavior against seismic wave. This relationship obtained by a logarithmic function is shown in Fig. 6. Using these equations, the multipliers of horizontal direction and vertical direction of the design-basis seismic floor response at the RV location are the obtained 7.2, 8.2, 9.3, 9.8 and 10 on horizontal direction and for 18.1, 22.5, 27.6, 29.8 and 31 on vertical direction respectively for 5, 5.5, 6, 6.2 and 6.3 of the multipliers of the input design-basis ground motion to the reactor building.

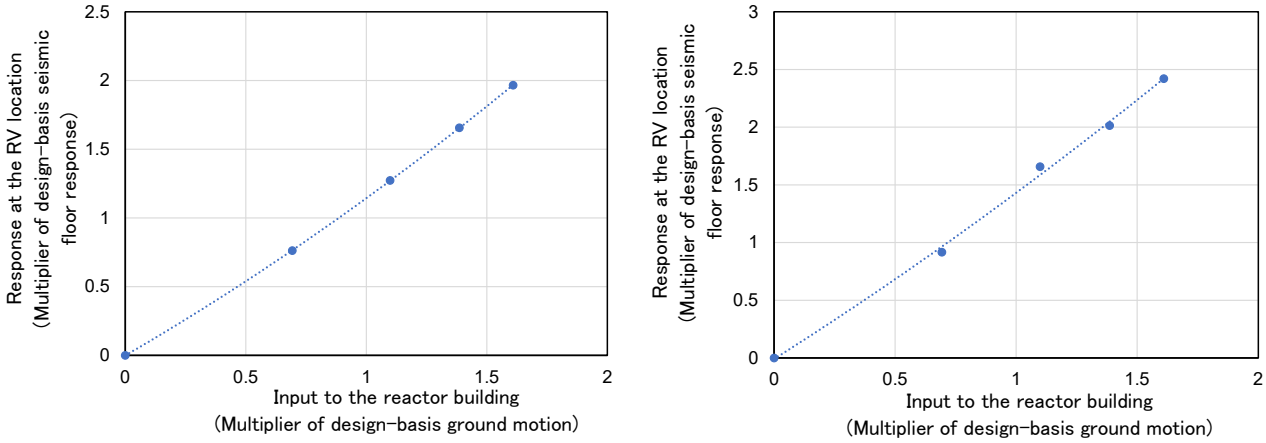

(a) Horizontal Direction (b) Vertical Direction

Figure 6. Relationship between the Input Seismic Ground Motion to the Reactor Building and the Seismic Floor Response at the RV Location

4.2 Deformation Behavior of the RV and Cumulative Fatigue Damage Fraction: Df

4.2.1 3-D structural analysis

Based on the conditions and the waveforms set up in Section 3, this study implemented the detailed three-dimensional structural analysis of the RV by a finite element method. Figure 7 and 8 show plastic strain contours calculated under the design-basis condition multiplied by a factor of 6.3. In this analysis, +X and +Y directions are represented as East and North, respectively. In these figures, four contours are presented from the view of the SE and NE directions for 80 s and 100 s. Structural deformation can be seen in Fig. 9 at the SE sides and Fig.10 from the top side, respectively, at around 80 s when the maximum absolute values of the strain of the vertical direction appeared. An axial compression type buckling can be seen at the upper part of the RV near the restraint position from Figs. 9 and 10, but this deformation does not reach the structure failure from a standpoint of maintaining the coolant boundary.

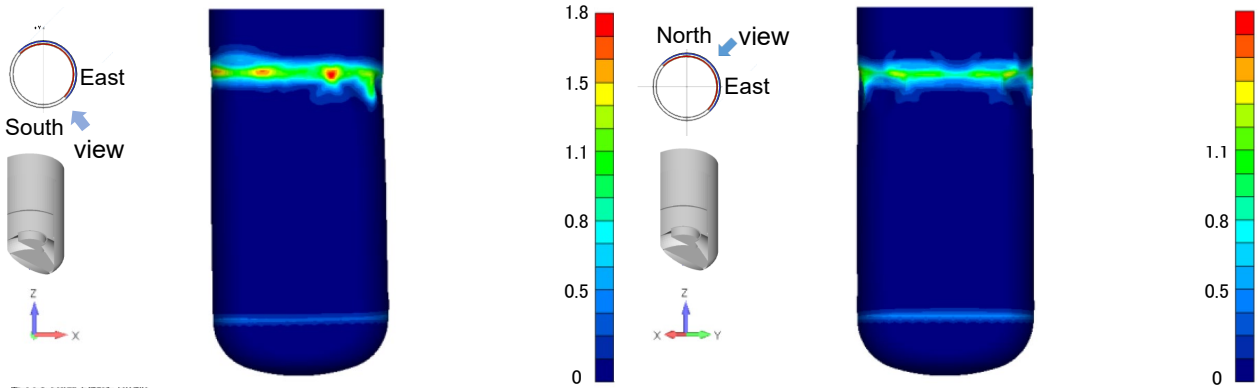

(a) View from SE Direction (b) View from NE Direction

Figure 7. Equivalent Plastic Strain Results at 80 s

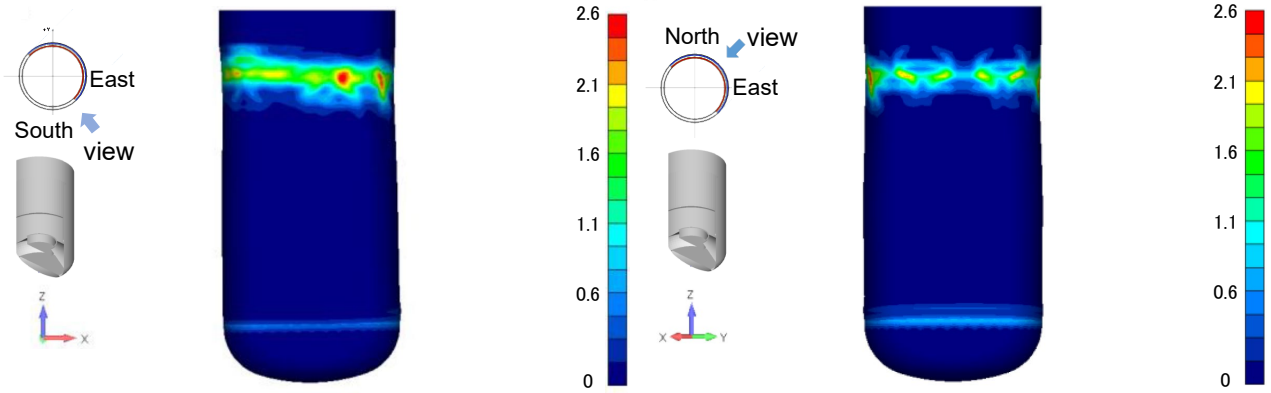

(a) View from SE Direction (b) View from NE Direction

Figure 8. Equivalent Plastic Strain Results at 100 s

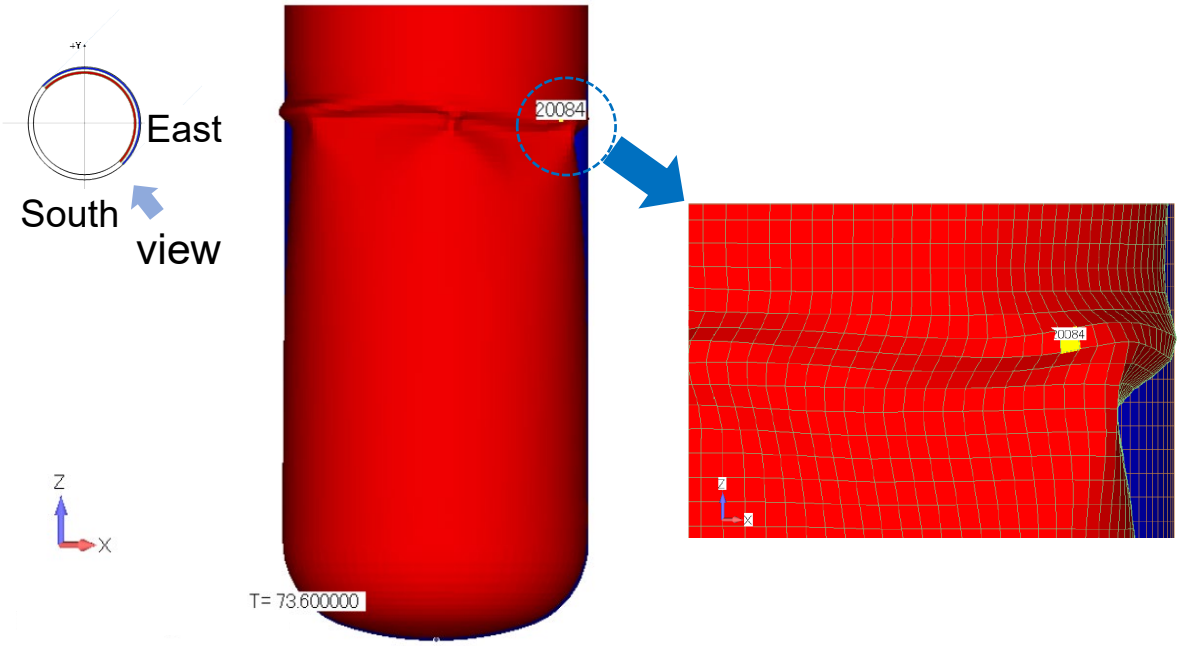

Figure 9. Structural Deformation Result at 73.6 s Viewed from the SE Side.

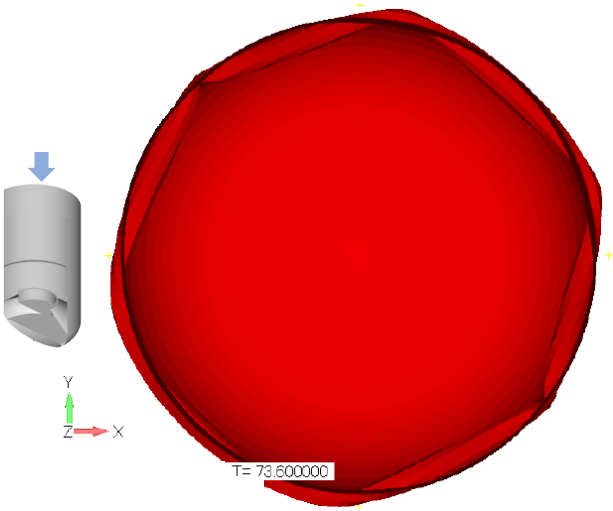

Figure 10. Structural Deformation Result at 73.6 s Viewed from the Top Side.

4.2.2 Cumulative fatigue damage fraction

The above-mentioned structural analysis calculated the time histories of the strain at various portions in the RV whole body. We focused on a local portion having the largest strain. Then the cumulative fatigue damage fraction: Df was evaluated by using the rainflow counting method [5] and best-fit fatigue failure equation [10]. Figure 11 shows the result of the evaluated Df. This study defines as RV failure when Df =1 or more. From the result, RV fails at 87s.

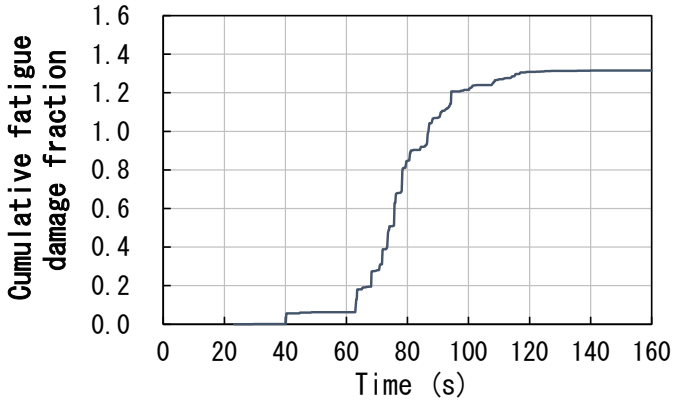

Figure 11. Cumulative Fatigue Damage Fraction at 6.3 Times to the Input Design-Basis Ground Motion to Reactor Building

4.2.3 Zooming analysis

This study implemented the zooming analysis as shown in Fig. 12 to evaluate in detail a local deformation at the buckled part in Figs. 9 and 10. In this zooming analysis, 1 element is subdivided into 3×3 meshes. Figure 13 shows comparison of time histories for the strain between the zooming analysis and the total area analysis in subsection 4.2.2. The former is larger than the latter. By using the calculated strain, Df is evaluated as Fig. 14 and Df calculated from the zooming analysis is also larger than that calculated from the total area analysis. Figure 14 indicates that RV fails at the time of 84 s because of Df =1. To evaluate RV fragility, this study adopted the Df value evaluated by the zooming analysis.

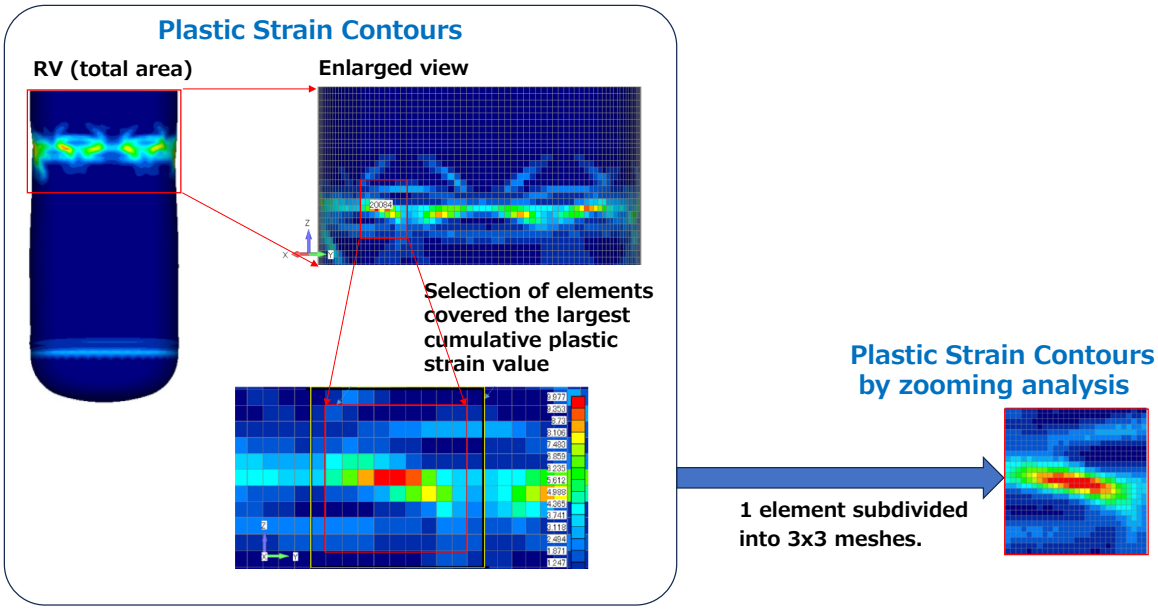

Figure 12. Zooming and Subdivision of Elements

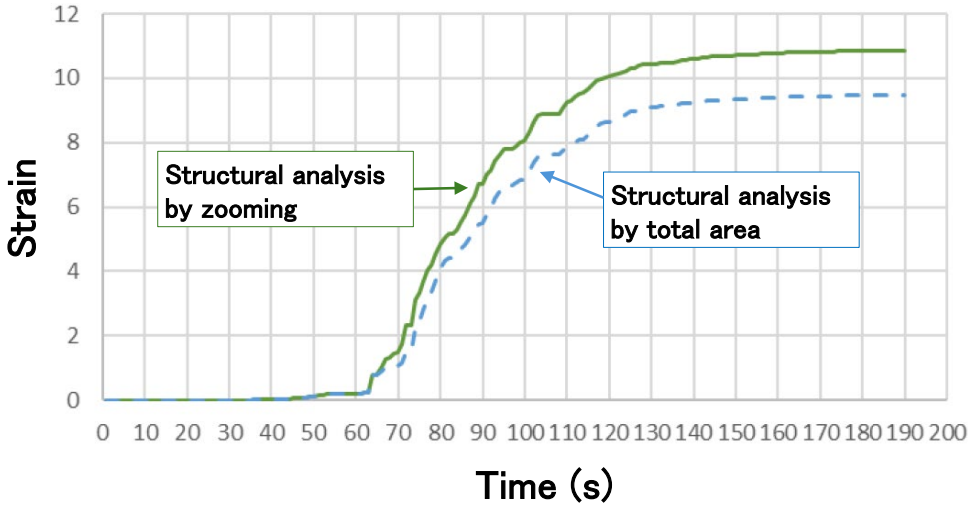

Figure 13. Time Histories for Strain

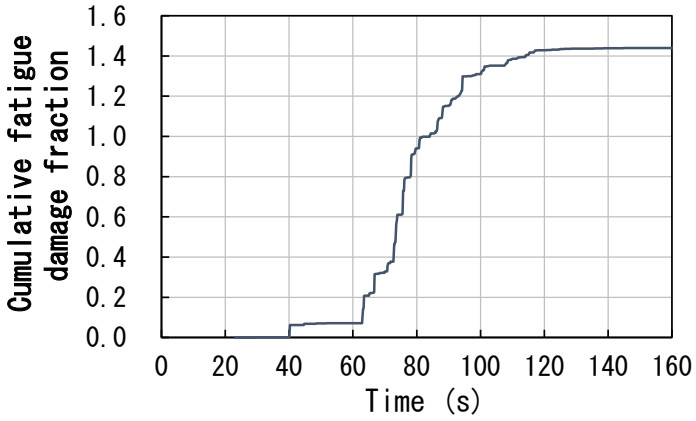

Figure 14. Cumulative Fatigue Damage Fraction at 6.3 Times to the Input Design-Basis Ground Motion to Reactor Building by Zooming Analysis

4.2.4 Cumulative fatigue damage fraction by zooming analysis

By the zooming analysis of section 4.2.3, the Df values are also evaluated for 5, 5.5, 6, 6.2 of the multipliers of input design-basis ground motion to the reactor building. The results are shown in Table 1.

Table 1. Summary of Df Values

Multipliers of input design-basis ground motion to the reactor building	Df value
5	4.46×10^{-4}
5.5	1.96×10^{-2}
6	1.92×10^{-1}
6.2	4.88×10^{-1}
6.3	$1.44 \times 10^{+0}$

5. FRAGILITY EVALUATION

To develop a fragility curve, this study applied the safety factor method [6] using response factor of the building and components, capacity factor and their uncertainties. The response factor of a reactor building includes the hardening effect of the seismic isolation system. The capacity factor is based on the buckling evaluation[7][8]. Since the buckling itself is not failure but deformation, the fatigue failure after the buckling is addressed for the fragility assessment in this study. The safety factors on the capacity factor are based on the buckling evaluation in the conventional buckling-based fragility evaluation, whereas this study considers that the safety factors on the capacity factor based on the buckling evaluation are replaced by the factors based on the fatigue damage evaluation. Using this method, this study developed the fragility curves on the basis of the conventional buckling-based and fatigue-based evaluations, which are presented in Fig. 15.

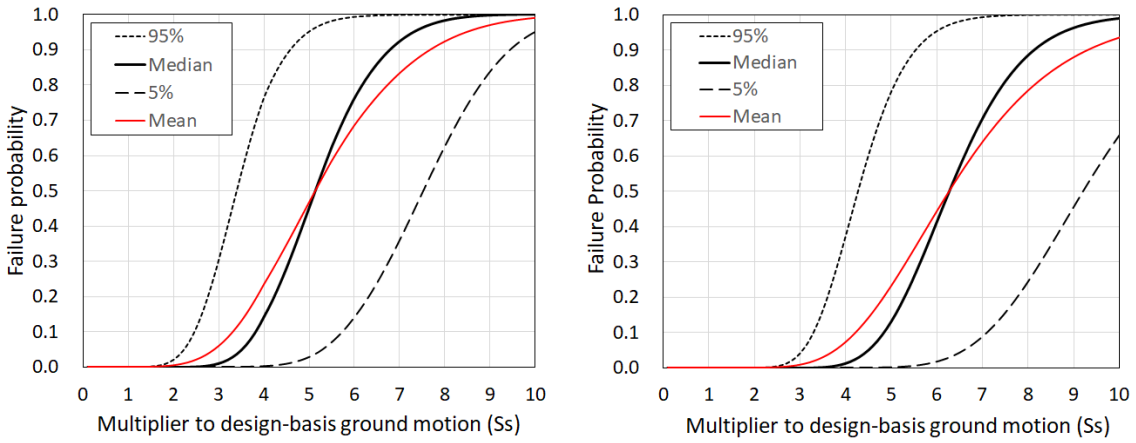

(a) RV Buckling Fragility (b) RV Post-Buckling Fatigue Failure Fragility

Figure 15. Comparison of RV Seismic Fragility between Different Failure Modes

For the fragility curves in Fig. 15, the values of the logarithmic standard deviation β_r of the aleatory uncertainty and β_u of the epistemic uncertainty were assumed to be based on the previous seismic PRA study [9]. However, β_r for the capacity factor of Df, which characterizes the RV post-buckling fatigue failure fragility in Fig.15, was determined by considering the variability of the RV material (i.e.; 316FR stainless steel) property which is associated with the best-fit fatigue failure equation [10]. These figures show the obtained fragility curves of 95%, 50% and 5% confidence level, and a mean fragility curve. The median value in the buckling-based evaluation is 5.2 of the multiplier of input design-basis ground motion to the reactor building. On the other hand, the median value in the fatigue-based evaluation is 6.3 of the multiplier, which shows 1.2 times higher than the buckling-based evaluation results of the conventional evaluation methodology. This analysis indicates that the fragility assessment developed in this study could contribute to improving the resilience of the nuclear structure.

6. SUPPRESSION OF HORIZONTAL DISPLACEMENT BY GUARD VESSEL AND RV FRAGILITY EVALUATION

The horizontal displacement for RV might be suppressed by contact with the GV, as shown in Fig.16. To evaluate the suppression effect for RV fragility, this study implements zooming analysis under the condition of the limit of the gap distance, where this study does not implement coupled analysis of RV and GV. For the zooming analysis, this study selects analysis cases (i.e., 6 and 6.3 of the multipliers of input design-basis ground motion to the reactor building) that horizontal displacement of RV is larger than gap distance of RV and GV. As result of the zooming analysis, the cumulative fatigue damage fractions are shown in Table 2 and results of fragility evaluation is shown in Fig.17. From the result, difference of two fragility curves was insignificant and it is not important to suppress of horizontal displacement for RV by contact with the GV in our model plant.

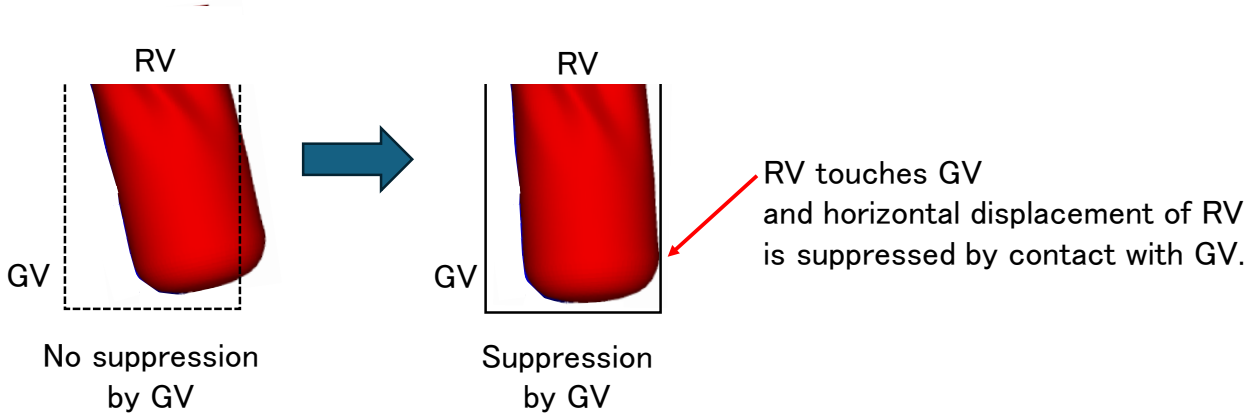

Figure 16. Illustration of Suppression of Horizontal Displacement for RV by Contact with the GV

Table 2. Df Values under the Condition of the Limit of the Gap Distance RV and GV

Multipliers of input design-basis ground motion to the reactor building	Df value	
	No suppression	Suppression
5	4.46×10^{-4}	
5.5	1.96×10^{-2}	
6	1.92×10^{-1}	1.77×10^{-1}
6.2	4.88×10^{-1}	
6.3	$1.44\times10^{+0}$	$1.20\times10^{+0}$

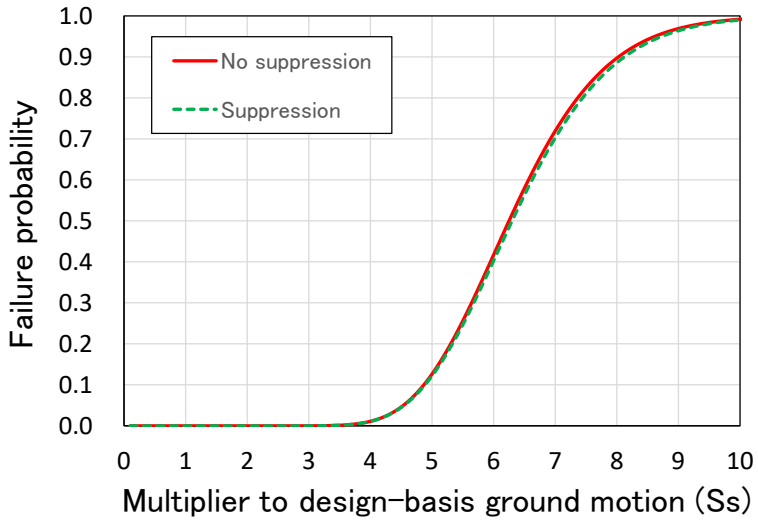

Figure 17. Comparison of RV Seismic Fragility between Suppression and no Suppression

7. CONCLUSION

In this study, the dynamic seismic structural analysis of the RV in the loop-type SFR using the FINAS/STAR code has shown the axial compression type buckling deformation at the upper part of RV near the restraint position under the excessive earthquake condition. Looking at the maximum cumulative strain position, this study calculated the cumulative fatigue failure fraction using the total strain. Using cumulative fatigue failure fractions, this paper developed the fragility curve using the safety factor method, which indicated the significantly improved curve compared the conventional buckling-based one. It can be concluded that the passive safety structure concept allows us to develop the fragility curve based on the fatigue without the unstable failure such as collapse under the excessive earthquake condition.

Acknowledgements

This work was supported by Ministry of Education, Sports, Science and Technology (MEXT) under Innovative Nuclear Research and Development Program Grant Number JPMXD0220353828. Special thanks to C. Jin, S. Sugaya, T. Kodama, W. Gu, S. Suzuki and Y. Nanazawa of ITOCHU Techno-Solutions Corporation for their assistance.

References

[1] Hidemasa Yamano, Satoshi Futagami, Masanori Ando and Kenichi Kurisaka, Development of failure mitigation technologies for improving resilience of nuclear structures, 6; Resilience improvements of fast reactors by failure mitigation for excessive earthquake, proceedings of Development of failure mitigation technologies for improving resilience of nuclear structures, 6; Resilience improvements of fast reactors by failure mitigation for excessive earthquake, Yokohama, Japan, March 3-8, 2024.

[2] The Japan Society of Mechanical Engineers. (2016). JSME Codes for Nuclear Power Generation Facilities -Rules for Design and Construction for Nuclear Power Plants -, Section II: Fast Reactor Standards, JSME S NC2-2016 (in Japanese).

[3] Uchida, M., Miyagawa, T., Murakami, H., Suzuno, T., Yamamoto, T. (2021). "A Study on Structures of Reactor Vessel of Pool-type Sodium-cooled Fast Reactor in case of adopted Three-Dimensional Isolation System," Transactions of 2021 Fall meeting in the Atomic Energy Society of Japan, (in Japanese).

[4] Kurisaka, K., Sakai, T., Yamano, H., Fujita, S., Minagawa, S., Yamaguchi, A., Takata, T. (2014). "Development of level-1 PSA method applicable to Japan Sodium-cooled Fast Reactor," Nuclear Engineering and Design, 269, 268–280. http://dx.doi.org/10.1016/j.nucengdes.2013.08.039

[5] M.Morishita et al., "A JSME code case on piping seismic design based on inelastic response analysis and strain-based fatigue criteria", Journal of Pressure Vessel Technology, 142, pp.021203-1 - 021203-14, (2020)

[6] Atomic Energy Society of Japan. (2015). AESJ Standards, A standard for Procedure of Seismic Probabilistic Risk Assessment for Nuclear Power Plants: 2015, AESJ-SC-P006E: 2015.

[7] Matsuura, S., Nakamura, H., Ogiso, S., Murakami, T., Kawamoto, Y. (1993). "Formulae for Evaluating Buckling Strength of FBR Main Vessels under Earthquake Loading," Japan Society of Mechanical Engineers (JSME) International Journal Series B Fluids and Thermal Engineering, 36(3), No.485-492.

[8] Matsuura, S., Nakamura, H., Murakami, T., Kawamoto, Y., Ogiso, S., Akiyama, H. (1994). "Studies on the Seismic Buckling Design Guideline of FBR Main Vessels. 2nd Report. Formulae for Evaluating Shear-Bending Buckling Strength," Transaction of Japan Society of Mechanical Engineers (Edition A), 60(575) No.93-1929 (in Japanese).

[9] Naruto, K., Nishino, H., Kurisaka, K., Yamano, H., Okano, Y., Okamura, S., Eto, M. (2014) "Seismic PRA for Japan sodium-cooled fast reactor (JSFR), Proc. 9th Korea-Japan symposium on nuclear thermal hydraulics and safety (NTHAS9), Buyeo, Korea, Nov. 16-19, No.9A0017.

[10] Shigeru Takaya, Naoto Sasaki, Masato Tomobe, Statistical properties of material strength for reliability evaluation of components of fast reactors; Austenitic stainless steels, https://doi.org/10.11484/jaea-data-code-2015-002 (in Japanese).